Role of MRI and MRS for the Study of Bone and Bone Marrow in Animal Models of Disease[§]

Felix W Wehrli
Laboratory for Structural NMR Imaging
University of Pennsylvania
Philadelphia, PA

Introduction

During recent years MRI has made significant inroads for the study of bone and bone marrow in both animals and humans. Even though, with conventional imaging pulse sequences, bone appears largely with background intensity, architecture of trabecular and cortical bone can be inferred from the image generated by the adjacent soft-tissues, notably the marrow in the endosteal cavity of long bones or vertebral bone marrow. MRI is clearly the modality of choice for studying the composition of marrow in terms of marrow adiposity, which changes in an age- and disease-specific manner, such as in response to treatment with steroids. Quantitative MRI techniques have also demonstrated potential for the study of marrow perfusion. While CT is perhaps preferable for structural studies of bone in animal models, MRI's strength is to provide information on architecture and soft-tissue properties simultaneously. Recent work also suggests that solid-state MRI techniques may provide unique information on bone water, matrix properties and mineralization, not amenable by other methods. While many of the technical developments during the past two decades have focused on skeletal applications in humans, the methodology is largely the same for the study in animal models, which is the topic of this presentation.

Trabecular and Cortical Bone Architecture

Trabecular thickness in various mammalian species ranges from about 30-50 μm in small rodents to 300 μm in cow bone. Quantitative imaging of trabecular bone (via imaging of marrow protons) thus requires high spatial resolution. The problem is exacerbated by bone's magnetic susceptibility, being more diamagnetic than either fatty or hematopoietic marrow by about 2.5-3ppm (S.I.) (1). The induced inhomogeneous field in the marrow spaces affects achievable image resolution, favoring spin-echo approaches (2).

Much of the early work was conducted ex vivo in specimens of rodent bone on high-field vertical-bore microimaging systems (3-5). Kapadia et al (4) first explored the potential of MR microscopy to the study of skeletal tissues at 400 MHz in excised intact proximal tibiae and coccygeal vertebrae of a young growing rat and an older retired female breeder rat at voxel sizes of 24x24x250 μm showing excellent correlation between of the MR-derived structural measures with histology. Weber et al (6) examined femurs of C57Bl/6 mice both in vivo and ex vivo at 11.7 T MRI scanner, followed by histologic processing and morphometry, finding good agreement between the two modalities as well as between in vivo and ex vivo MRI data for such parameters as bone volume fraction. Takahashi et al studied the short-term structural manifestations of steroid-induced osteoporosis in a rabbit model (7) as well as partial reversal upon discontinuation of corticosteroid exposure longitudinally in the same animals (8). Two-week treatment with subcutaneously administered dexamethasone induced a significant reduction in trabecular bone volume, which occurred at the expense of uniform trabecular thinning without affecting network architecture. The measurements were conducted at 1.5T in conjunction with custom-built RF coils. These data are the

[§] excerpted in part from *Comprehensive Biomaterials* (Ducheyne et al, eds.), Chap. 108 (Wehrli), Elsevier, 2011.

first to demonstrate the potential for studying the effects of drug intervention on skeletal parameters serially.

The quantitative characterization of trabecular architecture requires methods for digital processing of the images, notably techniques for segmentation and extraction of structural parameters, often based on stereologic principles developed for histomorphometry (9-11). Besides bone volume fraction and trabecular thickness, mean intercept length (MIL) is a parameter of interest. MIL is defined as the mean length between successive marrow intercepts along some chosen direction or averaged over all directions (12). Other approaches have focused on quantities that characterize topology (13) and structural orientation of the trabecular network (14). For example, it is known that during aging and osteoporotic bone loss a conversion of trabecular plates to rods takes place (15). Hildebrand et al conceived a parameter denoted structure-model index (SMI) (16) that is a measure of the bone's relative "platelikeness".

Also biomechanically relevant is structural orientation. Trabeculae grow and remodel in response to the direction and intensity of stresses to which it is subjected (Wolff's Law). Harrigan and Mann showed that the degree of orientation can be described in terms of a second-rank tensor (17). Chung et al, on the basis of 3D MR images of bovine and human trabecular bone specimens, showed that the approach furnishes the MIL and fabric tensor, characterized by three eigenvectors and three eigenvalues (10). They developed an algorithm for determining MIL as a function of direction from 3D volume images through parallel test lines across the imaging volume (**Figure 1**). It is clearly seen that the trabeculae are predominantly oriented along the axial direction (z-axis), which is the primary mechanical loading axis.

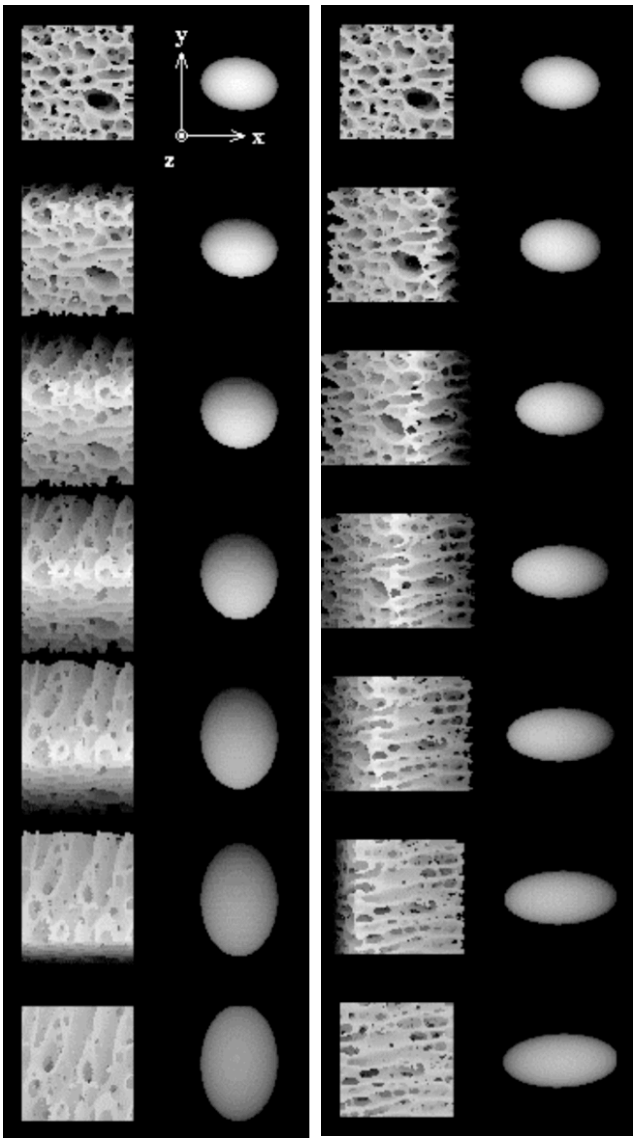

Figure 1 Volume-rendered projection MR images of a bovine tibia specimen, along with anisotropy ellipsoid (magnified thrice). The 7x7x7 mm^3 volume of interest is shown rotated in equal angular increments around a) x-axis, and b) y-axis. The z-axis approximately corresponds to the anatomic long axis of the tibia. (from Chung, et al, J Bone Min Res 10: 1452; 1995, adapted).

Bone Marrow

MRI and MRS are the modalities of choice for the study of bone marrow, in a broad spectrum of disorders, including infection, as well as neoplastic and degenerative disorders, in both animals and humans. The field is so vast that even cursory coverage is not possible. It suffices to point out that unlike any other method, MR can quantify marrow composition with great accuracy and precision, from simple

quantification of marrow adiposity by fat-selective imaging techniques (see, for example, (18)) to obtaining detailed information on fatty acid unsaturation by localized spectroscopy (19). As part of the study of the effects of corticosteroids on marrow composition discussed above, Takahashi et al studied the short-term temporal changes in marrow adiposity in response to dexamethasone in rabbits using spectroscopic imaging at 1.5T (7). The reduced marrow cellularity (conversion of hematopoietic to fatty marrow) at 2 and 4 weeks upon dexamethasone treatment is evidenced by the reduction in the intensity of the water signal. Further, whereas bone volume rapidly returned to baseline values upon discontinuation of dexamethasone exposure, the effect of marrow conversion turned out to be irreversible (8).

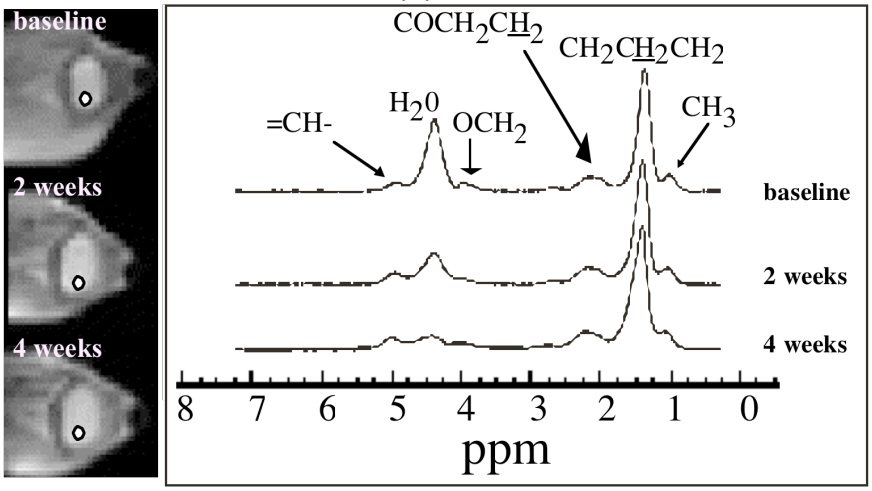

Figure 2: left: Transverse localizer images indicating location of the bone marrow proton spectra (2x2 pixel region of interest) in distal femoral metaphysis, obtained *in vivo* from the same animal at three time points. Spectral assignments correspond to water (H_2O) and triacylglyceride moieties. (From Takahashi et al, PNAS 2002)

Cortical Bone Water and Porosity

MRI and NMR spectroscopy can provide detailed insight into the nature of water in the various compartments of cortical bone (20-25). Water plays a key physiologic role by serving as a medium for transport of nutrients and waste products to and from osteocytes. Further, water at its various locations in the matrix, confers to bone its viscoelastic properties and its presence thus has important mechanical implications. Between 40 and 70% of the bone water, according to recent measurements in the author's laboratory, is bound to collagen of the osteoid, with the majority of the balance residing in the Haversian and Volkmann canals and a small portion occupying the osteocyte lacunae and canaliculi that interconnect osteocytes (26). Ong et al used deuterium NMR after extended immersion of specimens of rabbit and rat bone in D2O, thereby succeeding in separating collagen-bound from free (pore) water as the former exhibits quadrupole splittings (**Figure 3**).

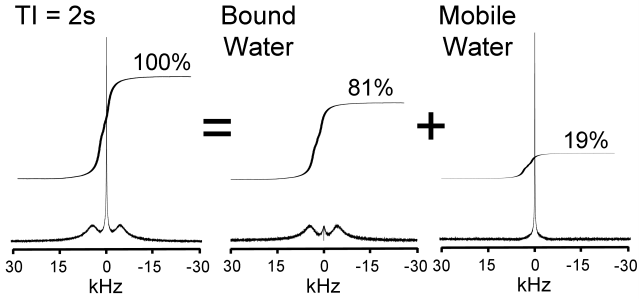

Figure 3. Sample ^{2}H spectra of sheep tibia cortical bone with relative integral areas. The mobile water component is suppressed in the center spectrum by inversion nulling, showing a deuterium splitting of ~8 kHz (Ong et al, ISMRM 2010).

More recently, Horch et al reported the results of a detailed analysis of the various proton signal components in cortical bone acquired at 4.7T on the basis of relaxation spectra obtained by Laplace inversion of FID and CPMG signals (27) (based on methodology conceived previously (21,22,28)). They were able to distinguish five micro-environments with the two major ones pertaining to collagen-

bound and pore water. Further, 2D T_2-T_2 relaxation exchange spectroscopy (REXSY) experiments from which the relaxation pools that are in exchange with each other can be identified, showing that the pool with the shortest lifetime (collagen protons, T_2~60μs) exchanged magnetization with a pool with T_2 ~400μs (presumably collagen-bound water) via magnetization transfer.

Fernandez et al studied transport kinetics of water in cortical bone by analyzing the exchange of the native water in specimens of rabbit cortical bone immersed in D_2O and monitoring the temporal increase of the proton H_2O signal in the D_2O bath (20). The integrated area of the water signal is thus proportional to the amount of water diffused from bone into the D_2O bath. Since the cortical bone samples were shaped as thin plates, the H_2O - D_2O exchange is dominated by diffusion perpendicular to the sample's largest surface, a situation for which an analytical solution exists. From the apparent diffusion coefficient (D_a = (7.8 ±1.5) x 10^{-7} cm^2/s) measured at 40°C (i.e. near physiological temperature), the authors concluded that diffusive transport of small molecules from the bone vascular system to the osteocytes occurs within minutes, values which are in good agreement with those obtained by Tate et al (29) by means of fluorescent tracers in rat bone.

Finally, Techawiboonwong et al developed a method for quantitative analysis of cortical bone water by means of ultra-short TE (UTE) imaging (30) in vivo in sheep and human bone (31,32). They showed that bone water concentration was significantly elevated in postmenopausal relative to premenopausal women with the largest increases noted in subjects with renal osteodystrophy (32). Du et al contributed substantially to the methodology for soft-tissue suppressed UTE imaging in terms of characterization of the detected short-T_2 protons in terms of their relaxation characteristics (33-36).

Solid-State MR Spectroscopy and Imaging of Bone Matrix and Mineral

The study of bone mineral chemistry has a long history and NMR spectroscopy has provided unique insight into this complex problem. Wet chemistry is problematic for this purpose since dissolution of the mineral into its ionic constituents provides limited information on the crystal structure of the calcium phosphates present in bone, typically regarded a nonstoichiometric calcium hydroxyapatite. During the past two decades ^{31}P and proton solid-state NMR, have provided new insight into bone mineral chemistry during growth, remodeling and in osteoporosis (37,38). Using two-dimensional solid-state ^{1}H - ^{31}P hetero-correlation NMR spectroscopy, researchers from the same laboratory determined the hydroxyl ion content in bone, variably reported previously as virtually absent, in spite of its presumed role as a constituent of the hydroxyapatite lattice (39). In a series of elegant experiments in which the authors examined mixtures of brushite and hydroxyapatite and also of bone from various species, they identified a resonance at 0.2ppm chemical shift that could be unambiguously assigned to the hydroxyl moiety since in this experiment the corresponding phosphorus signal results from cross-polarization via contact with the hydroxyl proton. **Figure 3** shows 2D solid-state ^{1}H - ^{31}P hetero-correlation NMR spectra of synthetic apatite showing characteristic cross peaks assigned to the hydroxyl proton and phosphate resonances.

Matrix and mineral constituents are also amenable to imaging by proton and ^{31}P solid-state MRI techniques. One of the first reports showing the capability to obtain 3D images of bone mineral is by Wu et al (40). The authors used a 3D radial projection imaging method in conjunction with nonselective radiofrequency pulses and quantification of phosphorus density was achieved by relating the image intensities to those in reference samples after adjusting for relaxation times. Comparison of the results with dual-energy X-ray absorptiometry (DXA), gravimetric and chemical analysis of calcium and phosphorus demonstrated the method to be quantitatively accurate.

Among the motivations for solid-state MRI as opposed to X-ray based densitometric

techniques are absence of ionizing radiation, beam hardening and other CT-specific artifacts. Further, the approach provides for direct measurement of a specific constituent of the mineral, thereby obviating reliance on assumptions about tissue composition. The latter is of particular importance for evaluating the two most common disorders of bone mineral homeostasis – osteoporosis and osteomalacia – which cannot be distinguished by densitometric techniques since both lead to loss of mineral, albeit via different mechanism. Osteomalacia is characterized by demineralization under volume retention whereas in osteoporosis bone volume is lost while the bone is generally normally mineralized. However, in order to quantify true mineralization, the tissue volume needs to be known. Cao et al developed and validated a solid-state ^{1}H MRI-based method in which protons from soft tissues are effectively suppressed, showing good agreement with independent measurements based on amino acid analysis and reference samples of known composition mimicking the properties of bone matrix protons (41). Anumula et al demonstrated the potential of high-field ^{31}P solid-state MRI and proton MRI in specimens of cortical bone from rabbits that had been subjected to a hypophosphatemic diet as a model for osteomalacia (42). A second group of animals was, after induction of osteomalacia in the above manner, returned to a normophosphatemic diet for some period to evaluate whether the loss in mineralization was reversible. As expected, osteomalacia lowered phosphorus density commensurate with a reduction in CT density and ultimate strength. However, these adverse effects on the bone's material and mechanical properties were largely reversible (**Figure 4**).

It is interesting that bone water (quantified in three different ways, by proton-deuteron exchange NMR as described previously (23), proton solid-state MRI and drying) showed the reverse behavior, i.e. increased water content in osteomalacic animals, commensurate with the notion that mineral and water densities are inversely related to one another (43).

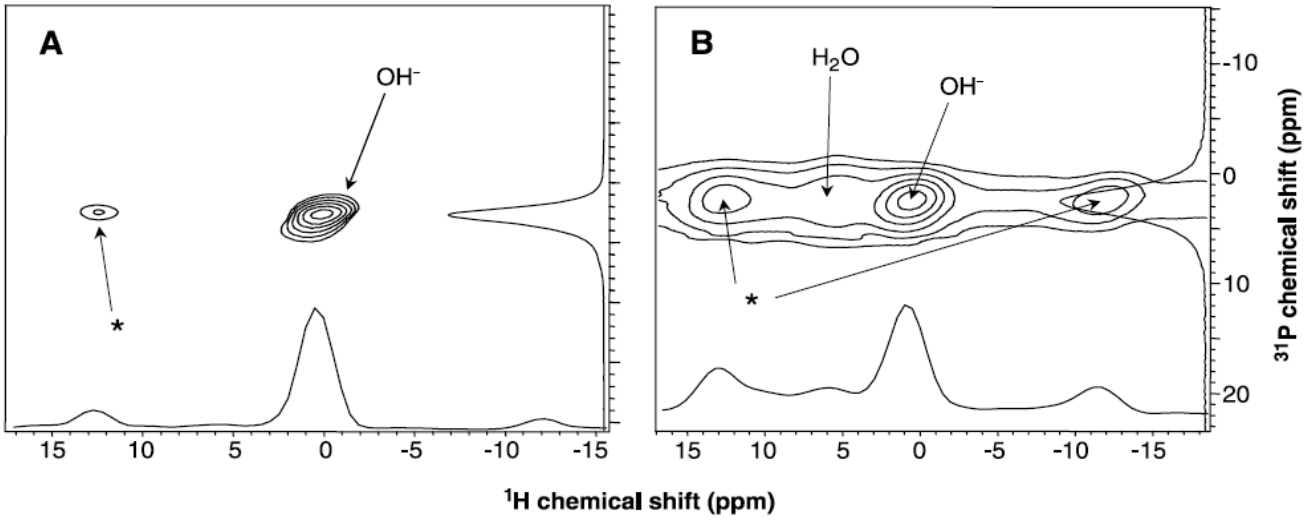

Figure 4 A) 2D ^{1}H-^{31}P hetero correlation NMR spectra of 95% hydroxyapatite/5% brushite at contact time = 0.3 ms; (B) bovine cortical bone at contact time = 0.2 ms. In both spectra, a prominent hydroxyl proton cross-peak is present. A weak water peak is also observed in the bone spectrum (reproduced from Cho et al, Science 300: 1123; 2003). Peaks marked with an asterisk are spinning sidebands.

There have been several reports providing evidence that rapid bone turnover as in ovariectomized rats or postmenopausal estrogen loss leads to decreased mineralization density, as quantified, for example, by microradiography (44) or synchrotron micro-CT (45) and that, conversely, antiresorptive treatment increases mineral density (44,46). In recent work from the author's laboratory, ^{31}P solid-state MRI performed in cortical bone from ovariectomized rats, showed a reduction in phosphorus density by 8% relative to sham-operated animals (25). Treatment with 25 μg/kg/day of alendronate for 50 days immediately after ovariectomy increased phosphorus density by 14% to values above those observed in sham-operated animals. Commensurate with these changes was increased bone water concentration in the ovariectomized animals, and loss after alendronate treatment.

References

1. Hopkins JA, Wehrli FW. Magnetic susceptibility measurement of insoluble solids by NMR: magnetic susceptibility of bone. Magnetic Resonance in Medicine 1997;**37**:494-500.
2. Ma J, Wehrli FW, Song HK. Fast 3D large-angle spin-echo imaging (3D FLASE). Magnetic Resonance in Medicine 1996;35:903-910.
3. Takahashi M, Wehrli FW, Wehrli SL, Hwang SN, Lundy MW, Hartke J, Borah B. Effect of prostaglandin and bisphosphonate on cancellous bone volume and structure in the ovariectomized rat studied by quantitative 3D NMR microscopy. Journal of Bone and Mineral Research 1999;14:680-689.
4. Kapadia RD, High WB, Soulleveld HA, Bertolini D, Sarkar SK. Magnetic resonance microscopy in rat skeletal research. Magn Reson Med 1993;30:247-250.
5. Gardner JR, Hess CP, Webb AG, Tsika RW, Dawson MJ, Gulani V. Magnetic resonance microscopy of morphological alterations in mouse trabecular bone structure under conditions of simulated microgravity. Magn Reason Med 2001;45:1122-1125.
6. Weber MH, Sharp JC, Latta P, Sramek M, Hassard HT, Orr FW. Magnetic resonance imaging of trabecular and cortical bone in mice: Comparison of high resolution in vivo and ex vivo MR images with corresponding histology. Eur J Rad 2005;53:96-102.
7. Takahashi M, Wehrli FW, Hilaire L, Zemel BS, Hwang SN. In vivo NMR microscopy allows short-term serial assessment of multiple skeletal implications of corticosteroid exposure. Proc Natl Acad Sci U S A 2002;19:19.
8. Takahashi M, Saha PK, Wehrli FW. Skeletal effects of short-term exposure to dexamethasone and response to risedronate treatment studied in vivo in rabbits by magnetic resonance micro-imaging and spectroscopy. J Bone Miner Metab 2006;24(6):467-475.
9. Chung HW, Wehrli FW, Williams JL, Kugelmass SD, Wehrli SL. Quantitative analysis of trabecular microstructure by 400 MHz nuclear magnetic resonance imaging. Journal of Bone and Mineral Research 1995;10(5):803-811.
10. Chung HW, Wehrli FW, Williams JL, Wehrli SL. Three-dimensional nuclear magnetic resonance microimaging of trabecular bone. Journal of Bone and Mineral Research 1995;10(10):1452-1461.
11. Majumdar S, Kothari M, Augat P, Newitt DC, Link TM, Lin JC, Lang T, Lu Y, Genant HK. High-resolution magnetic resonance imaging: three-dimensional trabecular bone architecture and biomechanical properties. Bone 1998;22(5):445-454.
12. Dalstra M, Huiskes R, Odgaard A, Van Erning L. Mechanical and textural properties of pelvic trabecular bone. Journal of Biomechanics 1993;26(4-5):523-535.
13. Saha PK, Gomberg BR, Wehrli FW. Three-dimensional digital topological characterization of cancellous bone architecture. International Journal of Imaging Systems and Technology 2000;11:81-90.
14. Odgaard A, Kabel J, van Rietbergen B, Dalstra M, Huiskes R. Fabric and elastic principal directions of cancellous bone are closely related. Journal of Biomechanics 1997;30:487-495.
15. Dempster DW, Birchman R, Xu R, Lindsay R, Shen V. Temporal changes in cancellous bone structure of rats immediately after ovariectomy. Bone 1995;16:157-161.
16. Hildebrand T, Laib A, Muller R, Dequeker J, Ruegsegger P. Direct three-dimensional morphometric analysis of human cancellous bone: microstructural data from spine, femur, iliac crest, and calcaneus. J Bone Miner Res 1999;14(7):1167-1174.
17. Harrigan TP, Mann RW. Characterization of Microstructural Anisotropy in Orthotropic Materials Using a Second Rank Tensor. Journal of Materials Science 1984;19:761-767.
18. Ma J. Dixon techniques for water and fat imaging. J Magn Reson Imaging 2008;28(3):543-558.

19. Ren J, Dimitrov I, Sherry AD, Malloy CR. Composition of adipose tissue and marrow fat in humans by 1H NMR at 7 Tesla. J Lipid Res 2008;49(9):2055-2062.
20. Fernandez-Seara M, Wehrli SL, Wehrli FW. Diffusion of exchangeable water in cortical bone studied by nuclear magnetic resonance. Biophysical Journal 2002;82:522–529.
21. Wang X, Ni Q. Determination of cortical bone porosity and pore size distribution using a low field pulsed NMR approach. J Orthop Res 2003;21(2):312-319.
22. Ni Q, King J, Wang X. The characterization of human compact bone structure changes by low-field nuclear magnetic resonance. Meas Sci Technol 2004(15):58–66.
23. Fernandez-Seara M, Wehrli SL, Takahashi M, Wehrli FW. Water content measured by proton-deuteron exchange NMR predicts bone mineral density and mechanical properties. J Bone Mineral Res 2004;19(2):289-296.
24. Wehrli FW, Fernandez-Seara MA. Nuclear magnetic resonance studies of bone water. Ann Biomed Eng 2005;33(1):79-86.
25. Anumula S, Wehrli SL, Magland J, Wright AC, Wehrli FW. Ultra-short echo-time MRI detects changes in bone mineralization and water content in OVX rat bone in response to alendronate treatment. Bone 2010;46(5):1391-1399.
26. Ong HH, Wright AC, Wehrli FW. Multiple Quantum NMR differentiates bound and mobile water in human cortical bone. 2010; Toronto, Ontario, Canada. J Bone Miner Res.
27. Horch RA, Nyman JS, Gochberg DF, Dortch RD, Does MD. Characterization of 1H NMR signal in human cortical bone for magnetic resonance imaging. Magn Reson Med;64(3):680-687.
28. Nyman JS, Ni Q, Nicolella DP, Wang X. Measurements of mobile and bound water by nuclear magnetic resonance correlate with mechanical properties of bone. Bone 2008;42(1):193-199.
29. Tate ML, Niederer P, Knothe U. In vivo tracer transport through the lacunocanalicular system of rat bone in an environment devoid of mechanical loading. Bone 1998;22(2):107-117.
30. Robson MD, Gatehouse PD, Bydder M, Bydder GM. Magnetic resonance: an introduction to ultrashort TE (UTE) imaging. J Comput Assist Tomogr 2003;27(6):825-846.
31. Techawiboonwong A, Song HK, Wehrli FW. In vivo MRI of submillisecond T(2) species with two-dimensional and three-dimensional radial sequences and applications to the measurement of cortical bone water. NMR Biomed 2007;21(1):59-70.
32. Techawiboonwong A, Song HK, Leonard MB, Wehrli FW. Cortical bone water: in vivo quantification with ultrashort echo-time MR imaging. Radiology 2008;248(3):824-833.
33. Du J, Hamilton G, Takahashi A, Bydder M, Chung CB. Ultrashort echo time spectroscopic imaging (UTESI) of cortical bone. Magn Reson Med 2007;58(5):1001-1009.
34. Du J, Takahashi AM, Bydder M, Chung CB, Bydder GM. Ultrashort TE imaging with off-resonance saturation contrast (UTE-OSC). Magn Reson Med 2009;62(2):527-531.
35. Du J, Takahashi AM, Bae WC, Chung CB, Bydder GM. Dual inversion recovery, ultrashort echo time (DIR UTE) imaging: creating high contrast for short-T(2) species. Magn Reson Med;63(2):447-455.
36. Du J, Carl M, Bydder M, Takahashi A, Chung CB, Bydder GM. Qualitative and quantitative ultrashort echo time (UTE) imaging of cortical bone. J Magn Reson;207(2):304-311.
37. Wu Y, Glimcher MJ, Rey C, Ackerman JL. A unique protonated phosphate group in bone mineral not present in synthetic calcium phosphates. Identification by phosphorus-31 solid state NMR spectroscopy. Journal of Molecular Biology 1994;244:423-435.
38. Wu Y, Ackerman JL, Kim HM, Rey C, Barroug A, Glimcher MJ. Nuclear magnetic resonance spin-spin relaxation of the crystals of bone, dental enamel, and synthetic hydroxyapatites. J Bone Miner Res 2002;17(3):472-480.
39. Cho G, Wu Y, Ackerman JL. Detection of hydroxyl ions in bone mineral by solid-state NMR spectroscopy. Science 2003;300(5622):1123-1127.
40. Wu Y, Ackerman JL, Chesler DA, Li J, Neer RM, Wang J, Glimcher MJ. Evaluation of bone mineral density using three-dimensional solid state phosphorus-31 NMR projection imaging. Calcif Tissue Int 1998;62(6):512-518.
41. Cao H, Ackerman JL, Hrovat MI, Graham L, Glimcher MJ, Wu Y. Quantitative bone matrix density measurement by water- and fat-suppressed proton projection MRI (WASPI) with polymer calibration phantoms. Magn Reson Med 2008;60(6):1433-1443.
42. Anumula S, Magland J, Wehrli SL, Ong H, Song HK, Wehrli FW. Multi-modality study of the compositional and mechanical implications of hypomineralization in a rabbit model of osteomalacia. Bone 2008;42(2):405-413.
43. Robinson RA, Elliot SR. The water content of bone. J Bone Joint Surg 1957;39A:167-188.
44. Boivin GY, Chavassieux PM, Santora AC, Yates J, Meunier PJ. Alendronate increases bone strength by increasing the mean degree of mineralization of bone tissue in osteoporotic women. Bone 2000;27(5):687-694.

45. Nuzzo S, Peyrin F, Cloetens P, Baruchel J, Boivin G. Quantification of the degree of mineralization of bone in three dimensions using synchrotron radiation microtomography. Med Phys 2002;29(11):2672-2681.
46. Roschger P, Rinnerthaler S, Yates J, Rodan GA, Fratzl P, Klaushofer K. Alendronate increases degree and uniformity of mineralization in cancellous bone and decreases the porosity in cortical bone of osteoporotic women. Bone 2001;29(2):185-191.